Catalysis Today 164 (2011) 353–357

Contents lists available at ScienceDirect

Catalysis Today

journal homepage: www.elsevier.com/locate/cattod

Semiconductor/reduced graphene oxide nanocomposites derived from photocatalytic reactions

Yun Hau Ng[a], Akihide Iwase[a], Nicholas J. Bell[a], Akihiko Kudo[b], Rose Amal[a,*]

[a] ARC Centre of Excellence for Functional Nanomaterials, School of Chemical Engineering, The University of New South Wales, Sydney, NSW 2052, Australia
[b] Department of Applied Chemistry, Faculty of Science, Tokyo University of Science, 1-3 Kagurazaka, Shinjuku-ku, Tokyo 162-8601, Japan

ARTICLE INFO

Article history:
Received 1 July 2010
Received in revised form 26 October 2010
Accepted 26 October 2010
Available online 4 December 2010

Keywords:
Reduced graphene oxide
Photocatalysis
Photoelectrochemical property

ABSTRACT

Graphene-based semiconductors nanocomposites were synthesized via a single-step photocatalytic reduction process. UV active titanium dioxide (TiO_2) and visible light driven photocatalysts (i.e. tungsten oxide (WO_3) and bismuth vanadates ($BiVO_4$)) with different conduction band energy levels were found efficient in transferring photogenerated electrons into graphene oxide (GO) thus reducing it to reduced graphene oxide (RGO). Simultaneously, nanocomposites of these particulate semiconductor and RGO sheet were obtained. X-ray photoelectron spectra revealed the 52–63% decrease in oxygen-containing carbon (hydroxyl and epoxy groups) of GO after illumination, indicating partial reduction of GO by excited photocatalysts. When made into thin films, photocurrent generation of these nanocomposites was enhanced by 160, 190 and 800%, respectively, for WO_3, TiO_2 and $BiVO_4$ as 5 wt% RGO was incorporated. These results demonstrate for the first time that a range of photocatalysts, not just TiO_2, can be used to reduce and incorporate GO into nanocomposites that have higher photoelectrocatalytic efficiencies than their parent materials.

1. Introduction

Graphene-based composite materials have attracted much attention as recent studies have shown their usefulness in electronics, photocatalysis and photovoltaic devices [1–3]. Graphene is able to enhance charge transport in a multitude of devices owing to its unique structure: an abundance of delocalized electrons within its conjugated sp^2-bonded graphitic carbon network enables graphene with excellent conductivity. To date, various metals–RGO and metal oxide–RGO nanocomposites including palladium, silver, gold, TiO_2, Co_3O_4 and CdSe particles have been reported [4–9]. Typically, these are synthesized using GO as the precursor followed by its reduction to partially restore the conductivity of the pristine graphene. These reduction methods of GO are in large extent dominated by chemical reduction using highly toxic hydrazine and hydrazine derivatives [10,11], thermal reduction [12], electrochemical reduction [13,14], solvothermal reduction [15] and sonolytic reduction [16]. Though effective, some of these methods are not energy and environmentally friendly as toxic substance and high temperature are required.

Recently, Kamat and co-workers have demonstrated an alternative reduction process involving UV-induced photocatalytic reduction of GO using TiO_2 nanoparticles [17]. The principle of this photocatalytic reduction lies on the ability of GO to undergo reduction when it accepts electrons from the excited TiO_2. As photocatalytic reaction does not require stringent experimental conditions such as involving toxic substances and higher temperature, it provides an alternative to prepare graphene-based composite in a greener and safer way. Since TiO_2 possesses highly negative conduction band energy, upon excitation with UV illumination, transfer of photogenerated electrons from their conduction bands to GO takes place efficiently. However, the applicability of the photocatalytic reduction of GO has not yet been proven in a wider context of photocatalysis as many visible light active photocatalysts are known for their much lower conduction band energy than the UV active TiO_2. Due to the weaker driving force to inject electrons from excited visible light photocatalysts such as WO_3 and $BiVO_4$ to GO, the effectiveness of these photocatalytic reactions has not been defined. Therefore, it is important to investigate this GO reduction under various photocatalytic systems to establish the genuineness of this method.

In this work, we present our studies on the utilization of a range of photocatalysts including visible light active WO_3, $BiVO_4$ and UV driven TiO_2 to study the effectiveness of GO photocatalytic reduction. X-ray photoelectron spectroscopy (XPS) studies

* Corresponding author. Tel.: +61 2 9385 4361; fax: +61 2 9385 5966.
E-mail address: r.amal@unsw.edu.au (R. Amal).

0920-5861/$ – see front matter © 2010 Elsevier B.V. All rights reserved.
doi:10.1016/j.cattod.2010.10.090

of the reaction products show that the photocatalytic reduction is as effective as existing reduction methods, with the advantage that it is a single-step, non-toxic reaction. The benefit of incorporating RGO to semiconductor in the application of photoelectrochemical cell is also demonstrated.

2. Experimental

2.1. Synthesis of GO and semiconductor/RGO composites

Graphite powder and WO_3 nanoparticles (<100 nm) were purchased from Aldrich; P25-type TiO_2 nanoparticles were supplied by Degussa. Other precursors for synthesizing $BiVO_4$ were obtained from Aldrich and Ajax Chemicals.

GO was prepared by a modified Hummers method [18]. One gram of graphite was added to a mixture of 23 cm^3 of concentrated H_2SO_4 and 500 mg of $NaNO_3$ in an ice bath. Three g of $KMnO_4$ was slowly added to the suspension to avoid any violent or explosive reactions. When all $KMnO_4$ was added, the dark green suspension was removed from the ice bath and slightly heated at 35–45 °C for an hour as grey-brown vapour evolved from the suspension. The mixture was diluted with 40 cm^3 of water. After completion of the reaction, 40 cm^3 of 10% H_2O_2 was added to the reaction vessel. The brown GO powder was filtered and washed at least twice with a mixture of 5% H_2SO_4 and 5% H_2O_2 and twice with distilled water. The GO was separated in the form of a dry brown powder. $BiVO_4$ was prepared by mixing 10 mmol of $Bi(NO_3)_3{\cdot}5H_2O$ and 5 mmol of V_2O_5 in 50 cm^3 of 0.75 M HNO_3 solution [19]. The suspension was stirred for two days at room temperature. The obtained greenish $BiVO_4$ was collected by filtration and dried at 110 °C. The synthesized $BiVO_4$ has a broader distribution of particle sizes ranged from ca. 300 to 600 nm.

Semiconductor powders (WO_3, $BiVO_4$ and TiO_2) were suspended in ethanol. GO with 5 wt% of the semiconductors was added to the suspension and sonicated for 30 min to produce a semiconductor-GO dispersion. The dispersion was then purged with nitrogen and exposed to either UV or visible light irradiation for 3 h through a water jacket using an Oriel 300 W xenon arc lamp to obtain semiconductor–RGO composites. The suspensions were stirred constantly during photoirradiation to ensure uniform illumination of the semiconductor–RGO during photocatalytic reduction. The resultant powder was sonicated in ethanol solution to obtain a 0.5 mg cm^{-3} concentration suspension and was drop-casted on the fluorine doped tin oxide (FTO) electrodes.

2.2. Characterizations (XPS, SEM, PEC)

X-ray photoelectron spectroscopy (XPS) measurements were performed using an ESCALab220i-XL probe (VG Scientific) with monochromated Al Kα radiation ($h\nu$ = 1486.6 eV). Analysis was carried out in a vacuum chamber (<2×10^{-9} mbar). Peak fittings and deconvolution were performed using the Eclipse (VG Scientific software). Scanning electron microscopy (SEM) images of the nanocomposites were obtained on a Hitachi S900 (4 kV) microscopes.

Photoelectrochemical measurements were carried out in a standard three compartment cell consisting of a working electrode, a Pt wire counter electrode, and a saturated Ag/AgCl reference electrode. N_2-saturated 0.1 M Na_2SO_4 or 1 M KOH were used as the electrolytes. A 300 W Xe lamp (Oriel) with or without 420 nm cut-off filter was used for excitation. An Autolab PGSTAT302N model potentiostat and its GPES programmer were employed for recording the *I*–*V* and amperometry signals.

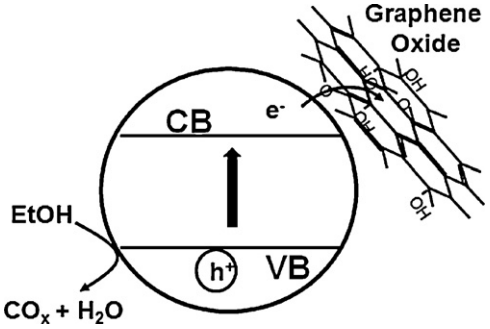

Scheme 1. Photocatalytic reduction of GO to RGO by a UV or visible light driven semiconductor.

3. Results and discussion

3.1. Photocatalytic reduction of graphene oxide by various photocatalysts

Scheme 1 demonstrates the basic principle behind the photocatalytic reduction of GO. Charge separation occurs in the de-aerated suspension of WO_3 and GO upon visible light illumination (>420 nm). Electrons stimulated into the conduction band are injected into GO as it comes into contact with WO_3, while holes in the valence band are scavenged by ethanol to produce ethoxy radicals, which are further oxidized to CO_2 and water. The direct physical interaction between WO_3 nanoparticles and GO sheets allows the in situ formation of WO_3–RGO nanocomposite after the reduction.

Fig. 1 shows the absorption spectra of WO_3–RGO recorded before and after 3 h illumination. The increase in overall absorption intensity after the irradiation in accordance with the change in the suspension color from light yellow to dark green, suggests the reduction of GO to RGO. This color change is a general observation during the reduction of GO and has been attributed to the partial restoration of the π-network within the graphitic carbon structure [10].

The C 1s X-ray photoelectron spectra of GO and photocatalytic reduced GO (WO_3–RGO) are shown in Fig. 2. Both samples clearly indicate three main carbon components that correspond to carbon atoms in different functional groups: the non-oxygenated C–C, C–O and the carboxylic C=O groups at 284.5, 286.6 and 288.9 eV, respectively. After 3 h irradiation, the ratio of peak intensity for C–O and C–C bonds in WO_3–RGO is substantially decreased compared to

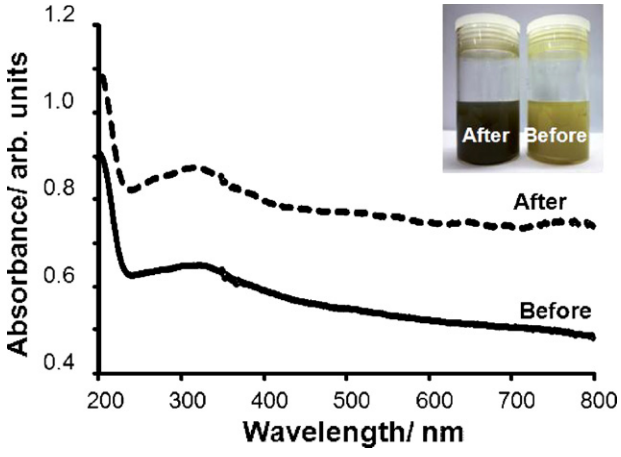

Fig. 1. Absorption spectra of WO_3–GO suspension before and after 3 h visible light illumination. Inset is the photographs of the respective suspensions.

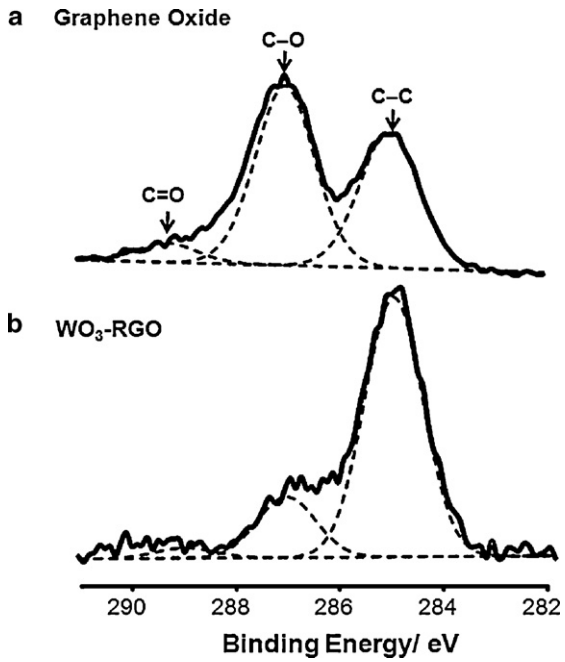

Fig. 2. C 1s XPS spectra of GO and WO_3–RGO.

that of the as-synthesized GO, suggesting the reduction of GO. Carboxylic groups (C=O) of GO, however, are almost un-affected after irradiation probably owing to its stability and strong interaction with surface hydroxyls of the semiconductor [20]. By comparing the area of graphitic peak (C–C) against the area of oxygen-containing groups (C–O and C=O), the degree of GO reduction by WO_3 is estimated to be 63%.

Table 1 indicates the percentage of C–C bonds and the ratio of peak area for C–C and C–O obtained on the commercial graphite, GO and RGO reduced by different photocatalysts under either visible light or UV illumination. Hummers method of graphite oxidation is very effective, the oxygen content in carbon increases from 8% for pure graphite (entry 1) to 59% for GO (entry 2) after the oxidation using a combination of strong oxidants like H_2SO_4, $KMnO_4$ and H_2O_2. In addition, Raman spectrum of the GO also demonstrated an increase in D band (1350 cm^{-1}) relative to its G band (1570 cm^{-1}) which indicates the increase amount of structural defect and dangling bonds of the sp^2 carbon that break the symmetry of pristine graphene as the result of graphite oxidation (data not shown). Insignificant changes in the amount of oxygen-containing groups of GO after UV illumination in the absence of photocatalysts have excluded the direct photoreduction of GO (entry 3). Therefore the reduction of GO must be attributed to the photocatalytic reaction of the semiconducting nanoparticles.

As reported by others [17,21,22], various UV-active photocatalysts have been found effective in reducing GO to RGO and these include both anatase and rutile TiO_2, ZnO and $SrTiO_3$. These photocatalysts share the common ground of having energetic conduction band positions, i.e. conduction band position < 0 eV vs NHE at pH 0. The electron transfer from these photocatalysts to GO is therefore anticipated, though precise reduction potential of GO has not been reported [13]. In this work, TiO_2 is found to regenerate the C–C species to 74% (entry 4). This value is as effective as compared with 68 and 77% of C–C restoration using hydrazine and hydrazine-assisted annealing reduction of GO [23]. Furthermore, introduction of nitrogen containing species (C–N bonds) to the RGO in the common hydrazine reduction technique as indicated in XPS analysis is effectively avoided using a photocatalytic reduction [24]. In contrast, WO_3 and $BiVO_4$ are generally regarded as photocatalysts with weak reducing power owing to their positive conduction band position (conduction band position > 0 eV vs NHE at pH 0) which prohibits the electron transfer to reduce H_2O to H_2 [25,26]. These photocatalysts are in general employed as O_2-photocatalysts to oxidize H_2O to O_2 in the presence of electrons scavenger. Interestingly, 78 and 71% of the C–C bonds are restored in the WO_3–RGO (entry 5) and $BiVO_4$–RGO (entry 6) samples, respectively, after visible illumination. The ability of WO_3 and $BiVO_4$ to effectively reduce GO to a degree which is comparable to those reduced by UV-active TiO_2 or chemical reducing agent, proves even the visible light photocatalyst can be used to prepare graphene-based composites. It provides a greener and safer alternative in processing graphene-based materials.

Table 1
Degree of GO reduction calculated from the ratio of C–C/C–O XPS peak areas.

Entry	Sample	Ratio of C–C/C–O	Total of C–C, %
1	Graphite	12.60	92
2	GO (as synthesized)	0.76	41
3	GO (UV irradiated)	0.88	44
4	TiO_2–RGO	3.55	74
5	WO_3–RGO	4.30	78
6	$BiVO_4$–RGO	3.20	71

3.2. Photoelectrochemical behaviour of semiconductor–RGO photoelectrodes

After the completion of photocatalytic reduction process, suspension of the semiconductor–RGO with a typical concentration of 0.5 g cm^{-3} was fabricated into thin films by drop-casting the solutions onto fluorinated tin oxide-coated slides. Typical film densities of ~2 mg cm^{-2} were achieved over areas of approximately 3 cm^3. Fig. 3(a)–(c) shows the morphology of photocatalysts–RGO composite under a field-emission SEM microscope. The morphological features of all samples are essentially identical, except for the intrinsic difference in the size of the parent particles. Carboxylic species of the GO interacts with the surface hydroxyl groups of the photocatalysts particles enables the dispersion and adhesion of particles on GO and the subsequent obtained RGO flakes. As can be seen in the SEM images, RGO flakes are decorated with the photocatalysts particles and its translucence indicates the nature of its thinness, though single layers of RGO sheets are not achieved. It is reasonable to imagine that such a structure would enable easy charge transfer between the particles and the RGO sheets. From the perspective of photocatalyst–RGO contact quality, TiO_2 with the smallest individual particles (~30–50 nm) should have the largest contact surface with RGO, followed by the WO_3 (<100 nm) and $BiVO_4$ (~500 nm). Although high-quality photocatalyst–RGO contact is important in boosting charge transfer from the particles to RGO flakes, in an electrode-type application, however, there is another crucial factor that determines the final electrons that flow through the circuit, i.e. the contact between FTO and photocatalyst particles. Crystallinity of all photocatalysts before and after incorporation of RGO in an illuminating process remains unchanged, as indicated from the XRD and Raman spectroscopy analyses (data not shown). This ensures a valid comparison in studying the effect of RGO in photoelectrochemical measurements.

The photocurrent generated by these RGO incorporated semiconductor thin films was measured using a standard three-compartment electrochemical cell, with the film as the photoanode. Upon illumination of light with energy greater than its band gap, photocatalyst particles undergo charge separation to yield electrons and holes. As the holes are presumably scavenged by OH^- ions or consumed by other organics in the electrolyte, the electrons are collected by the FTO electrode to generate photocurrent. Under visible light, photocurrent of ~11 and 8 μA cm^{-2} was obtained

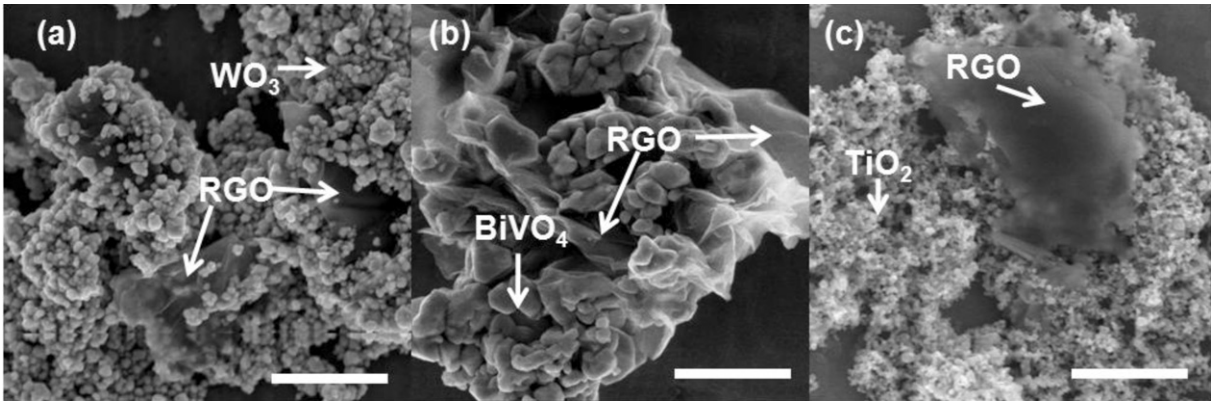

Fig. 3. SEM images of (a) WO_3–RGO, (b) $BiVO_4$–RGO and (c) TiO_2–RGO composites. Scale bars correspond to 1 μm.

using pure WO_3 and $BiVO_4$, respectively, while ~20 μA cm^{-2} was observed on TiO_2 under UV illumination, as shown in Fig. 4. When 5 wt% RGO was incorporated into these photocatalyst particles using the photocatalytic process described earlier, these numbers jumped to ~18, ~65 and ~40 μA cm^{-2}, respectively, corresponding to photocurrent increases of 160, 800 and 190%. These photocurrent enhancements clearly demonstrate the constructive effect of RGO in boosting the electrons transport of pristine photocatalyst particulate thin films. Although net photocurrents obtained from the electrodes were relatively low in this work, our previous studies have shown that the incident photon to current efficiency (IPCE) of the system is comparable to the other literature works [27,28]. Net photocurrent generation of the electrodes could be improved by various strategies, include annealing the electrodes at higher temperature, modifying the electrode fabrication method and even applying incident light with higher intensity. Besides, the difference in the degree of photocurrent enhancement is believed to be mainly due to the quality of contact between nanocomposite and FTO substrate [29]. WO_3 and TiO_2 employed in this work have the smaller particles (<100 nm) than that of the larger $BiVO_4$ (~500 nm). The smaller size of the WO_3 and TiO_2 particles affords a larger contact area with the FTO substrate, and therefore better charge transfer ability. The $BiVO_4$ particles, being much larger, contact a much smaller area of the FTO electrode. The addition of RGO to the $BiVO_4$ film likely adds many more conduction pathways between $BiVO_4$ and FTO, dramatically enhancing the current flow. Therefore, when the two dimensional RGO sheets are introduced, the extent of its effect in improving the contact is much obvious in the case of $BiVO_4$. We confirmed this hypothesis by fabricating particles of WO_3 with larger diameters of 150–180 nm and comparing the photocurrent generated by films of these particles with and without RGO. Adding 5 wt% RGO to the nanoparticle film boosted the photocurrent by 270%. This factor possibly explained the greater photocurrent enhancement in $BiVO_4$ than that of WO_3 and TiO_2 with the presence of RGO. Note that this photocurrent enhancement is yet to be optimized by the amount of RGO incorporation. Our separate work revealed the dependence of photocurrent generation on the quantity of RGO present in the system [26].

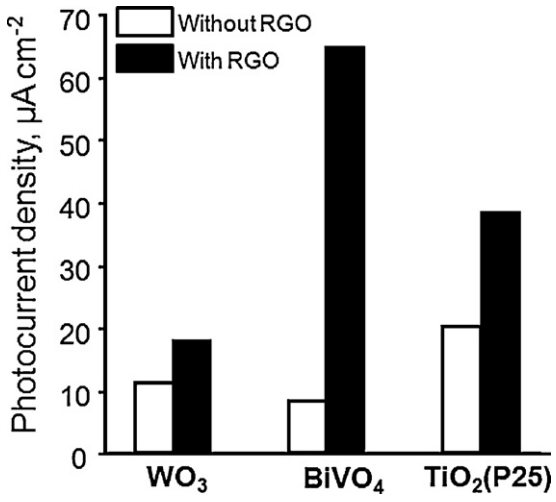

Fig. 4. Comparison of photocurrent generation among various semiconductors with and without the presence of RGO. Photocurrents were recorded at 0.75 V in 0.1 M Na_2SO_4 for WO_3 and $BiVO_4$ while TiO_2 was measured at 0 V in 1 M KOH.

In general, charge trapping sites within the photocatalyst particulate network annihilate the photogenerated electrons, therefore, limiting its collection efficiency at the FTO electrode. Charge recombination is promoted by the existence of many grain boundaries among the particles. Loss of the vast majority of charge carriers occurs during the electrons diffusion across the countless recombination centers. Poor contact between the particles and FTO electrode further worsen the electron transport. The comprehensive integration of RGO into these particulate systems introduces a second conduction network within the film that has a lower resistance than the nanoparticle network itself. Electrons are injected to RGO immediately after their generation at the surface of photocatalyst particles. This greatly reduces the likelihood of electrons to encounter trapping sites prior to reaching the FTO electrode. Electrons injected to RGO are then quickly shuttled to the FTO collecting electrode through the large pool of delocalized electrons from its conjugated π–π graphitic carbon network. The improvement in electron transport in this system is also evident in the elongated electrons lifetime of $BiVO_4$ in a separate photocurrent relaxation analysis [28].

4. Conclusions

The results presented in this study proved the feasibility of using photocatalytic reaction to reduce graphene oxide. A wide range of photocatalysts include both UV and visible light triggered photocatalysts has been employed to reduce graphene oxide while simultaneously incorporating it into the nanoparticle agglomerates to create photocatalyst–RGO nanocomposite. Restoration of C–C bonds of graphene oxide upon illuminated with WO_3, $BiVO_4$ and TiO_2 were determined to be 71–78% and the values are comparable to the reported chemical reduction of graphene oxide by toxic hydrazine or high temperature annealing. Furthermore, absence of the unwanted C–N species as introduced by hydrazine-induced reduction of graphene oxide again proved the advantage of using the photocatalytic reduction. When these RGO incorporated pho-

tocatalyst particles were employed as thin film photoanodes in an electrochemical cell, the generated photocurrent was improved by between 160 and 800% compared to that of pure semiconductor films alone. The boost is due to the RGO providing a low resistance conduction pathway through the nanoparticle matrix as well as better contact between the nanoparticle film and the FTO substrate. As these phenomena were observed in all systems in this work, the practicability of RGO to enhance electrons transport in photocatalyst particles is proven and may find use in wider applications in photocatalysis.

Acknowledgements

The authors thank the Australian Research Council for its financial support to the project. Y.H. Ng thanks Prof. Prashant V. Kamat from the University of Notre Dame, USA, for assistance and advice in establishing the experimental procedures. Dr. Bill Bin Gong is gratefully acknowledged for his help in XPS measurement and analysis.

References

[1] P.V. Kamat, J. Phys. Chem. Lett. 1 (2010) 520–527.
[2] H. Zhang, X. Lv, Y. Li, Y. Wang, J. Li, ACS Nano 4 (2010) 380–386.
[3] S.R. Kim, M.K. Parvez, M. Chhowalla, Chem. Phys. Lett. 483 (2009) 124–127.
[4] G.M. Scheuermann, L. Rumi, P. Steurer, W. Bannwarth, R. Mulhaupt, JACS 131 (2009) 8262–8270.
[5] R. Pasricha, S. Gupta, A.K. Srivastava, Small 5 (2009) 2253–2259.
[6] R. Muszynski, B. Seger, P.V. Kamat, J. Phys. Chem. C 112 (2008) 5263–5266.
[7] T.N. Lambert, C.A. Chavez, B. Hernandez-Sanchez, P. Lu, N.S. Bell, A. Ambrosini, T. Friedman, T.J. Boyle, D.R. Wheeler, D.L. Huber, J. Phys. Chem. C 113 (2009) 19812–19823.
[8] Z-S. Wu, W. Ren, L. Wen, L. Gao, J. Zhao, Z. Chen, G. Zhou, F. Li, H.-M. Cheng, ACS Nano 4 (2010) 3187–3194.
[9] Y. Lin, K. Zhang, W. Chen, Y. Liu, Z. Geng, J. Zeng, N. Pan, L. Yan, X. Wang, J.G. Hou, ACS Nano 4 (2010) 3033–3038.
[10] S. Stankovich, D.A. Dikin, R.D. Piner, K.A. Kohlhaas, A. Kleinhammes, Y. Jia, Y. Wu, S.T. Nguyen, R.S. Ruoff, Carbon 45 (2007) 1558–1565.
[11] S. Stankovich, D.A. Dikin, G.H.B. Dommett, K.A. Kohlhaas, E.J. Zimney, E.A. Stach, R.D. Piner, S.T. Nguyen, R.S. Ruoff, Nature 442 (2006) 282–286.
[12] H.C. Schniepp, J.-L. Li, M.J. McAllister, H. Sai, M. Herrera-Alonso, D.H. Adamson, R.K. Prud'homme, R. Car, D.A. Saville, I.A. Aksay, J. Phys. Chem. B 110 (2006) 8535–8539.
[13] H.-L. Guo, X.-F. Wang, Q.-Y. Qian, F.-B. Wang, X.-H. Xia, ACS Nano 3 (2010) 2653–2659.
[14] S.J. An, Y. Zhu, S.H. Lee, M.D. Stoller, T. Emilsson, S. Park, A. Velamakanni, J. An, R.S. Ruoff, J. Phys. Chem. Lett. 1 (2010) 1259–1263.
[15] H. Wang, J.T. Robinson, X. Li, H. Dai, J. Am. Chem. Soc. 131 (2009) 9910–9911.
[16] K. Vinodgopal, B. Neppolian, I.V. Lightcap, F. Grieser, M. Ashokkumar, P.V. Kamat, J. Phys. Chem. Lett. 1 (2010) 1987–1993.
[17] G. Williams, B. Seger, P.V. Kamat, ACS Nano 2 (2008) 1487–1491.
[18] W.S. Hummers, R.E. Offeman, J. Am. Chem. Soc. 80 (1958) 1339.
[19] A. Iwase, H. Kato, A. Kudo, J. Sol. Energy Eng. 132 (2010) 021106.
[20] T.J. Meyer, G.J. Meyer, B.W. Pfennig, J.R. Schoonover, C.J. Timpson, J.F. Wall, C. Kobusch, X. Chen, B.M. Peek, C.G. Wall, W. Ou, B.W. Erickson, C.A. Bignozzi, Inorg. Chem. 33 (1994) 3952–3964.
[21] G. Williams, P.V. Kamat, Langmuir 25 (2009) 13869–13873.
[22] Y.H. Ng, A. Iwase, R. Amal, unpublished results.
[23] H.A. Becerril, J. Mao, Z. Liu, R.M. Stoltenberg, Z. Bao, Y. Chen, ACS Nano 2 (2008) 463–470.
[24] S. Stankovich, R.D. Piner, X. Chen, N. Wu, S.T. Nguyen, R.S. Ruoff, J. Mater. Chem. 16 (2006) 155–158.
[25] R. Abe, T. Takata, H. Sugihara, K. Domen, Chem. Commun. (2005) 3829–3831.
[26] A. Kudo, K. Omori, H. Kato, JACS 121 (1999) 11459–11467.
[27] Y.H. Ng, I.V. Lightcap, K. Goodwin, M. Matsumura, P.V. Kamat, J. Phys. Chem. Lett. 1 (2010) 2222–2227.
[28] Y.H. Ng, A. Iwase, A. Kudo, R. Amal, J. Phys. Chem. Lett. 1 (2010) 2607–2612.
[29] A. Iwase, A. Kudo, J. Mater. Chem. 20 (2010) 7536–7542.